Chemical Engineering Journal 259 (2015) 257–265

Contents lists available at ScienceDirect

Chemical Engineering Journal

journal homepage: www.elsevier.com/locate/cej

Selective removal of Hg(II) with polyacrylonitrile-2-amino-1,3,4-thiadiazole chelating resin: Batch and column study

Chunhua Xiong [a,*], Yanli Li [a], Guotao Wang [a], Lei Fang [b], Suguo Zhou [a], Caiping Yao [a], Qing Chen [a], Xuming Zheng [c], Dongming Qi [d], Yaqin Fu [d], Yaofeng Zhu [d]

[a] Department of Applied Chemistry, Zhejiang Gongshang University, Hangzhou 310012, China
[b] Department of Food Science and Human Nutrition, University of Florida, Bldg 475 Newell Drive, Gainesville, FL 32611, USA
[c] Engineering Research Center for Eco-Dyeing & Finishing of Textiles, Ministry of Education, Zhejiang Sci-Tech University, Hangzhou City, Zhejiang Province 310018, China
[d] School of Materials and Textile, Zhejiang Sci-Tech University, Hangzhou City, Zhejiang Province 310018, China

HIGHLIGHTS

- A novel chelating resin of PAN-ATD was synthesized via one-step reaction.
- PAN-ATD exhibited good overall adsorption properties and could be easily eluted to Hg(II).
- High adsorption capacity and selectivity are attributed to the nitrogen groups.
- PAN-ATD can be potentially used in waste treatment and detection area.

ARTICLE INFO

Article history:
Received 26 May 2014
Received in revised form 26 July 2014
Accepted 28 July 2014
Available online 9 August 2014

Keywords:
Chelating resin
Polyacrylonitrile
Adsorption
Hg(II)
FT-IR

ABSTRACT

A novel chelating resin, polyacrylonitrile-2-amino-1,3,4-thiadiazole (PAN-ATD), was prepared via one-step reaction and its structure was characterized by elemental analysis and FT-IR. The adsorption properties of the resin for Hg(II) were investigated by batch and column experiments. Batch adsorption results showed that PAN-ATD had high affinity towards Hg(II) and the maximum adsorption capacity estimated from the Langmuir model was 526.9 mg/g at 308 K. The adsorption kinetic and equilibrium data were well fitted to the pseudo-second-order model and the Langmuir isotherm model, respectively. Furthermore, the resin can be easily regenerated and reused with less than 10% loss of adsorption capacity. Also, the resin and its metal complexes were studied by SEM, TGA, and energy dispersive X-ray spectroscopy (EDS). With good overall properties (a high selectivity adsorption capacity, easy to be regenerated and stable application capacity) PAN-ATD resin can not only be used in selective removal of Hg(II) from waste solution, but also be used for preparation of the separation and enrichment column applied in the analysis and detection area.

1. Introduction

Heavy metal contamination is becoming one of the main concerns of environmentalists due to their non-biodegradability and high toxicity even at trace concentrations [1]. Mercury, as one of the important heavy metals, is released to the environment from wastewater such as paper, oil refinery, pulp, chlor-alkali manufacturing, pharmaceutical, and battery manufacturing industries [2]. Exposure to mercury can damage the nervous system in humans, especially for the developing nervous system of young children [3]. Hence, removing heavy metals from wastewater to reduce its hazards is a critical task in the perspective of environment and health.

Various technologies have been applied in removing mercury from industrial effluents, among which some are expensive, inefficient or polluting, such as solvent extraction, reduction, coagulation, reverse osmosis, chemical precipitation, membrane separation, and ion exchange [4,5]. In contrast, adsorption is regarded as a guaranteed and practical treatment method by utilizing its low cost, high adsorption capacity, easy metal recovery and good reusability. And a wide range of materials can be used to remove mercury from solutions such as chitosan [5], activated carbon [6],

* Corresponding author. Address: No. 149 Jiaogong Road, Hangzhou 310012, China. Tel.: +86 0571 88071024x7571.
E-mail address: xiongch@163.com (C. Xiong).

http://dx.doi.org/10.1016/j.cej.2014.07.114
1385-8947/

carbon nanotubes [7,8], Pumice-supported nanoscale [9], guar gum [10], silica nanocomposite [11,12], aluminosilicates [13], polythioamides [14,15], MCM-41 [16], zinc oxide nanoparticles [17], barley husk silica [18], magnetite (Fe_3O_4) particles [19], and polyacrylonitrile [20–22]. Polyacrylonitrile (PAN) is an ideal polymeric matrix with a series of merits such as solvent resistance, thermal and mechanical stability, abrasion resistance, and high tensile strength [22]. Active nitrile groups (C≡N) in PAN can easily be converted into a number of new functional groups via special reactions. Deng et al. [20,21] used the aminated polyacrylonitrile fibers to remove copper, lead, and chromium ions from aqueous solutions, but the metal adsorption capacity was not very ideal. Our initial report suggested that the 2-aminothiazole functionalized polyacrylonitrile resin containing nitrogen and sulfur atoms can be used for selective adsorption of Hg(II) from solutions with a good adsorption capacity [22].

In this work, as a continuation of our initial work, we design another novel chelating resin (PAN-ATD) by grafting 2-amino-1,3,4-thiadiazole (ATD for short) on the surface of polyacrylonitrile beads. The synthetic resin was characterized by FT-IR, elemental analysis, TGA and DSC. The adsorption capability for Hg(II) in the aqueous solution had been investigated by a series of batch and column experiments. To further understand the adsorption process, the adsorption kinetics, isotherms and the thermodynamic properties of the adsorption of Hg(II) on the synthetic resin were also clarified. The recovery of Hg(II) and reusability of the adsorbents were also studied in detail.

2. Materials and methods

2.1. Materials and chemicals

Mesoporous-type cross-linked polyacrylonitrile beads (PAN), cross-linked with 7% divinylbenzene (DVB), nitrogen content 22.18%, functional groups content 15.83 CN mmol/g, specific surface area 27.8 m^2/g, pore size 25.1 nm, were purchased from Chen Guang Chemical Industrial Institute of China. Aqueous solutions of ions at various concentrations were prepared from $NiSO_4{\cdot}6H_2O$, $HgCl_2$, $CuCl_2{\cdot}2H_2O$, $Zn(NO_3)_2{\cdot}6H_2O$, $Cd(NO_3)_2{\cdot}4H_2O$, and $Pb(NO_3)_2$ and were used as sources for Ni(II), Hg(II), Cu(II), Zn(II), Cd(II), and Pb(II), respectively. All other reagents and solvents were of analytical grade and used as received without further purification.

2.2. Measurements

FT-IR spectra were scanned in the region of 400–4000 cm^{-1} in KBr pellets on NICOLET 380 FT-IR spectrophotometer. C, N, and S elements were analyzed by a Vario EL III Elemental Analyzer. The specific surface area and the mean pore size of the resins were determined on an Autosorb-1 automatic surface area and pore size analyzer. Thermogravimetric analysis in a range of temperature 50–1000 °C by 20 °C min^{-1} under the protection of nitrogen on a TGA instrument; Differential scanning calorimeter (DSC) was recorded on a HCR-1 DSC under N^2 atmosphere (20 cm^3 min^{-1}) at 20 °C min^{-1}. The shapes and surface morphology of the resins were observed by means of a HITACHI S-3000N scanning electron microscope (SEM), in conjunction with SEM imaging. The elemental compositions of the resins were analyzed by energy-dispersive spectrometer (EDS). The concentrations of Hg(II) and the coexistent metal ions were determined by Perkin Elemer Optima 2100DV inductively coupled plasma optical emission spectrometer (ICP-OES). The respective zeta potentials of PAN-ATD resins were determined by a zeta potential analyzer (Malvern Zetasizer Nano ZS90). The sample was shaken in the DSHZ-300A temperature constant shaking machine. Mettler Toledo delta 320 pH meter was used for pH measurement.

2.3. Preparation of PAN–ATD

The preparation procedure is simple and described as follows: 0.5 g of PAN beads and 300 mL of *N*,*N*-dimethylformamide (DMF) were added into a 500 mL three-neck round-bottom flask, swelling over night. Then, 3.20 g of ATD (molar ratio of reagent (ATD/PAN) = 4) and a small amount of metallic sodium used as catalyst were added to the flask. The mixture reacted for 14 h at 140 °C with 100 rpm stirring speed under a nitrogen atmosphere. The solid product was carefully washed thoroughly with DMF and deionized and then with acetone and ether. After that the obtained resin was dried in vacuum at 50 °C. The conversion of the functional group of the synthetic resin can be calculated from sulfur content by the following equations:

$$F_c = \frac{S_c}{32.07 \times n_s} \times 1000 \quad (1)$$

$$x = \frac{F_c \times 1000}{F_0 \times 1000 - F_c \times M_L \times F_0} \quad (2)$$

where F_0 (15.83 mmol of CN/g) and F_c are the contents of the functional group of polyacrylonitrile and the resin synthesized, respectively, x is the functional group conversion (%), M_L is molar mass of the ligands (mol/g), n_s is the number of sulfur atoms of ligand molecules, and S_c is the sulfur content of the synthetic resin (%).

2.4. Batch adsorption experiments

Batch experiments were carried out to investigate the Hg(II) adsorption property on the prepared PAN-ATD resin by placing 15.0 mg resin in a series of flasks containing 30 mL of the studied metal ions at the desired initial concentration and pH. Then the contents of the flasks were shaken in a flask-shaker at specific temperature for a given time with a speed of 100 rpm. The residual concentration of the studied metal ions in the solution was determined by ICP. The adsorption capacity (Q, mg/g) and distribution coefficient (D, mL/g) were calculated with the following expression:

$$Q = \frac{C_0 - C_e}{W} V \quad (3)$$

$$D = \frac{C_0 - C_e}{W C_e} V \quad (4)$$

where C_0 is the initial concentration of Hg(II) (mg/mL), C_e is the residual concentration of Hg(II) in solution (mg/mL), V is the solution volume (mL), and W is the resin dry weight (g). The above batch adsorption experiments for the adsorption of Hg(II) by PAN-ATD in aqueous solutions were performed at different pH values, contact times, initial concentrations of Hg(II) and temperatures. The operating variables studied for the extent of adsorption were pH, contact time, initial concentration and temperature.

2.5. Column adsorption experiments

Column experiments were carried out in a fixed-bed mini glass column (Φ3 mm × 30 cm) under the optimum pH 6.5 obtained from the batch experiments at a constant temperature of 298 K, which is close to the environmentally relevant conditions. Then, 100.0 mg PAN-ATD was presoaked in the column for 24 h before the experiment began. In order to avoid the channeling of the effluent, a certain concentration of Hg(II) solution in a constant flow rate was passed continuously through the stationary bed of sorbent in up-flow mode. The outgoing Hg(II) concentration was determined at different time intervals as described above.

2.6. Desorption and regeneration

After adsorption, resins were collected, and gently washed with distilled water to remove any unabsorbed metal ions. Then, the resin was agitated with 30 mL of HCl solution and HNO_3 solution (0.5–4.0 mol/L), at 100 rpm for 24 h at 298 K. The final concentration of Hg(II) in the aqueous phase was measured. After each adsorption–desorption cycle, the resin beads were washed and regenerated and then used for the next cycle adsorption. The desorption ratio (E) was calculated as follows:

$$E(\%) = \frac{C_d V_d}{(C_0 - C_e)V} \times 100\% \quad (5)$$

where C_d is the concentration of Hg(II) in the eluent solutions, V_d is the volume of the desorption solution, C_0, C_e, and V are the same as defined above.

3. Results and discussion

3.1. Characterization of PAN–ATD

The structures of PAN, ATD, and PAN-ATD were confirmed by FT-IR spectroscopy. Fig. 1 shows the FT-IR spectra of PAN with characteristic peaks at 2243 cm^{-1} related to C≡N groups, 2933, 2873, 1452 cm^{-1} related to the antisymmetric stretching vibration band, symmetric stretching vibration band, and bending vibration band of $-CH_2$ groups, respectively. The adsorption bands at 3288 and 3316 cm^{-1} are assigned to the $-NH_2$ group in ATD. Comparing the PAN and ATD spectra, the remarkable decrease in peak intensity and a slight shift from 2243 to 2239 cm^{-1} of C≡N band, the disappearance of the stretching vibrations of $-NH_2$ group at 3288 and 3316 cm^{-1}, along with the appearance of a new band at 3392 cm^{-1} related to secondary amino group (–N–H) in the spectra of PAN and ATD, indicated that the reaction between C≡N and $-NH_2$ occurred and the ATD ligands have been grafted onto the PAN polymer surface successfully. The characteristics and elemental analysis of the resin are shown in Table 1. The specific surface area and mean pore size are slightly changed after grafting of ATD with PAN. The increase of N content and the new appearance of S content confirmed the grafting of ATD ligands on the surface of the PAN polymer. The functional group capacity of the newly synthetic resin (PAN-ATD) was 3.55 mmol obtained from the elementary analysis of sulfur, and the functional group conversion was 34.92%. The potential synthesis routes of PAN-ATD resin is presented in Scheme 1 on the basis of the FT-IR analysis. The thermal behavior of the prepared PAN-ATD was evaluated by TGA and DSC. As seen in Fig. 2, The slight weight loss before 200 °C may be attributed to the emitted water and volatile materials, a further weight loss from 200 to 400 °C, resulting from the decomposition of ATD grafted to PAN, after that a sharp weight loss occurred at 400–520 °C along with exothermic peak corresponding to degradation of the remaining polyacrylonitrile chains, which is in close to the report by Kiani et al. [23].

The FT-IR spectra of the Hg(II) adsorbed resin (PAN-ATD-Hg) was also revealed to find out the adsorption mechanism. In the spectra of PAN-ATD-Hg (Fig. 1), the stretching vibration of –N–H peak was shifted from 3392 to 3435 cm^{-1}, the bending vibration of N–H peak at 1582 cm^{-1} disappeared. In addition, the stretching vibration of C–N shifted from 1251 to 1239 cm^{-1}, the peak at 1619 cm^{-1} related to C=N in the heterocyclic and 1667 cm^{-1} related to —C=NH disappeared, while a new broad peak at 1605 cm^{-1} appeared, indicating that the nitrogens in –N–H, C–N, C=N and —C=NH are involved in chelation adsorption of Hg(II). The peak of C–S at 711 cm^{-1} remain, however, unchanged after

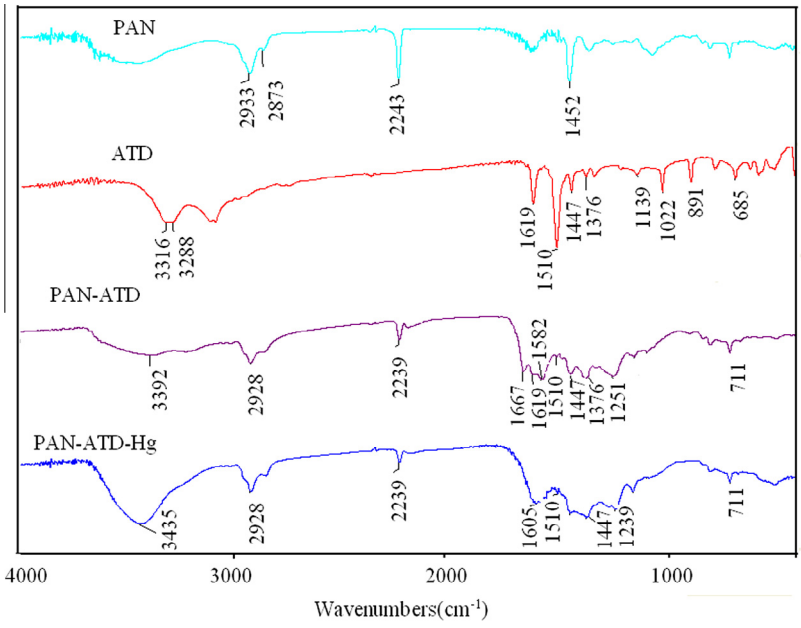

Fig. 1. FT-IR spectra of PAN, ATD, PAN-ATD and PAN-ATD-Hg.

Table 1
Characteristics and elemental analysis data of the resin.

	N content (%)	S content (%)	Functional group content	Functional group conversion (%)	Specific surf. area (m^2/g)	Mean pore size (nm)
PAN	22.18		15.83 CN mmol/g		27.80	25.1
PAN–ATD	14.37	11.38	3.55 ATD mmol/g	34.92	27.83	25.4

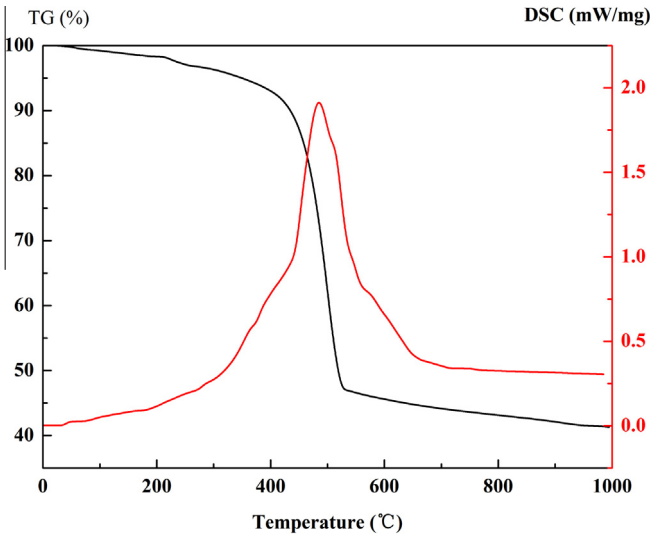

Fig. 2. TGA-DSC curves of PAN-ATD.

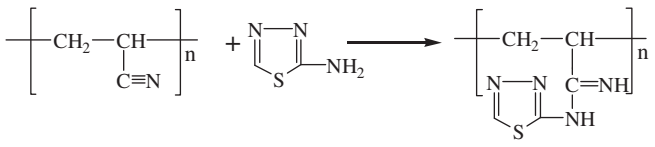

Scheme 1. Synthesis routes for PAN-ATD.

adsorption of Hg(II), suggesting that the endocyclic sulfur is not involved in coordination [24].

3.2. Effect of pH

Initial solution pH can seriously influence the adsorption process by affecting the formation of the metal ions and the surface properties of the adsorbents, then impact the adsorption amount. To avoid the hydrolysis of metal ions, the effect of pH on adsorption of Hg(II) was studied at a pH range of 2.5–6.5 at 298 K. The results obtained were presented in Fig. 3, and it can be seen that the adsorption capacity of Hg(II) on PAN-ATD increased with the pH rising from 2.5 to 6.5 and reached to the maximum value of 456.1 mg/g at the pH value of 6.5. According to Dong et al. [25], the dominant Hg(II) species is $HgCl_2$ at pH < 3 and $Hg(OH)_2$ at pH > 4. At pH of 2.5–3.5, PAN-ATD was positively charged as their pHzpc (3.4 ± 0.1, Fig. S1) was higher than solution pH, less uptake of Hg(II) occurred at this pH values, was attributed to the subgroup of PAN-ATD that played the major role in binding Hg(II),–N–H, was protonated and the competition of H^+ with Hg(II) for the active sites decreased the adsorption capacity [26]. At pH ⩾ 4 $Hg(OH)_2$ was the dominant species, and –N–H and –C=N–H on PAN-ATD became deprotonated (–N^- and —C=N^-), which may complex with $Hg(OH)_2$, forming –NHg^+ and C=NHg^+ [27]. According to the Pearson theory, the $Hg(OH)_2$ is more softer than Hg(II) and the C=N group with a very soft basic has a superior affinity with $Hg(OH)_2$ at pH range 3.5–6.5, which also attributed to the higher adsorption capacity at this pH range.

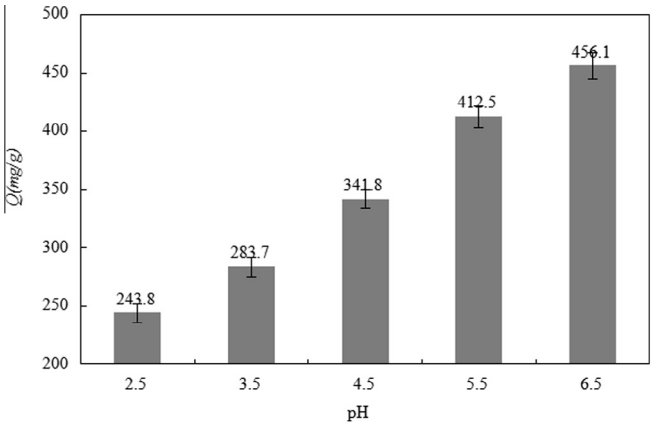

Fig. 3. Effect of pH on the adsorption capability of PAN-ATD for Hg(II) (resin 15.0 mg, initial metal ion concentration = 10.0 mg/30.0 mL, pH 2.5–6.5, T = 298 K, 100 rpm).

3.3. Selective adsorption behaviors

The selective adsorption property for Hg(II) was also investigated in a mixed metal solution containing Hg(II) and the Ni(II), Cu(II), Cd(II), Pb(II), and Zn(II) metal ions in the same pH range, the results was shown in Fig. 4. It can clearly be found that PAN-ATD adsorbed much more Hg(II) than the other metal ions in the entire pH range of study, indicating that PAN-ATD exhibits a higher selectivity adsorption for Hg(II). The high selective coefficients of PAN-ATD for Hg(II) in different pH were obtained by using the following equation: selective coefficient = Q/Q', where Q (mg/g) is the adsorption capacity of Hg(II) in the mixed metal solution system, and the Q' (mg/g) is the total adsorption capacity of the other metal ions in the mixed metal solution. The results were shown in Table 2. Since the process of removing toxic metals is usually carried out in a mixed metal ions system, the high selectivity of PAN-ATD for Hg(II) at pH 2.5–6.5 is a matter of practical importance and Hg(II) can be easily removed from these meta matrix. The high

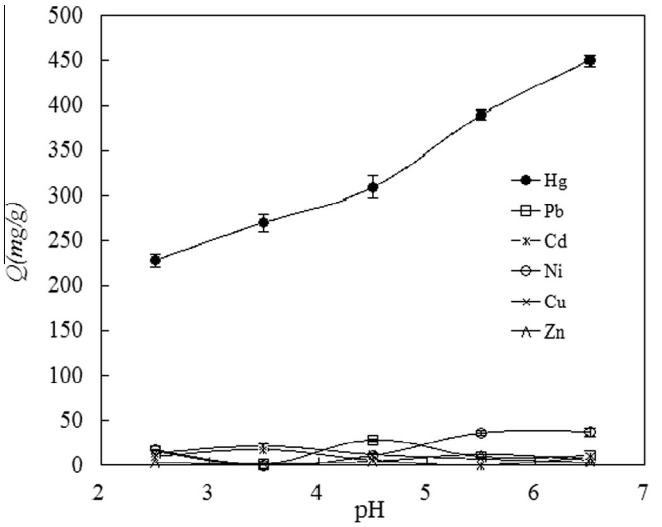

Fig. 4. Adsorption capacities of the PAN-ATD for Hg(II), Pb(II), Cd(II), Ni(II), Cu(II), and Zn(II) (resin 15.0 mg, initial metal ion concentration = 10.0 mg/30.0 mL, pH 2.5–6.5, T = 298 K, 100 rpm).

Table 2
Adsorption selectivity of PAN-ATD for Hg(II).

pH	2.5	3.5	4.5	5.5	6.5
Selective coefficient	3.75	5.14	7.01	8.96	12.48

adsorption capacity and selectivity for Hg(II) result from the different nitrogen groups in the PAN-ATD that show different affinities to Hg(II) and the Ni(II), Cu(II), Cd(II), Pb(II), and Zn(II) metal ions. The –N–H group contributes to the high adsorption capacity toward Hg(II), and the C=N group contributes to the high selectivity toward Hg(II), because it is a very soft basic and has a superior affinity with Hg(II) ions [28–30].

3.4. Effect of contact time and temperature

The effect of contact time and temperature on the Hg(II) adsorption process were investigated in the time range of 1–50 h under pH 6.5 at 288, 298, and 308 K. As seen in Fig. 5, Hg(II) adsorption capacity increased rapidly in the first 10 h and then slowed down until the equilibrium state was reached. The less time needed to reach the equilibrium state and the higher adsorption capacity at higher temperature are due to the greater swelling of the resin and increased diffusion of metal ions into the resin at a higher temperature, which indicated the adsorption of Hg(II) onto PAN-ATD was more effective at higher temperatures.

3.5. Kinetics of adsorption

The results described in the "Effect of contact time and temperature" section were used to further investigate the kinetic mechanism that controls the adsorption process. Pseudo-first-order, pseudo-second-order, and Elovich kinetic models shown as Eqs. (6)–(8) [31–33] were tested to interpret the experimental data:

$$\log(Q_e - Q_t) = \log Q_1 - \frac{k_1}{2.303}t \tag{6}$$

$$\frac{t}{Q_t} = \frac{1}{k_2 Q_2^2} + \frac{t}{Q_2} \tag{7}$$

$$Q_t = \frac{1}{\beta}\ln(\alpha\beta) + \frac{1}{\beta}\ln t \tag{8}$$

where Q_e and Q_t are adsorption capacities at equilibrium and at any time t (mg/g), Q_1 and Q_2 are the calculated adsorption capacities of the pseudo-first-order model and the pseudo-second-order model (mg/g), respectively, k_1 and k_2 are the rate constants of the pseudo-first-order model (h^{-1}), and the pseudo-second-order model (g/(mg h)), α (mg/g min) is the initial adsorption rate and β (g/mg) is an indication of the number of sites available for the adsorption and relevant with the extent of surface coverage and activation energy for chemisorption. The kinetic parameters obtained from Eqs. (6)–(8) are represented in Table 3. The extreme high value of correlation coefficients (>0.999), along with well fit to the calculated Q with experimental data, indicates that the adsorption process can be best explained by pseudo-second-order mechanism. This suggests that the rate-limiting step of Hg(II) ion onto PAN-ATD is chemisorption, where valency forces are involved via electrons sharing or exchange between the resin and the Hg(II) ions [34].

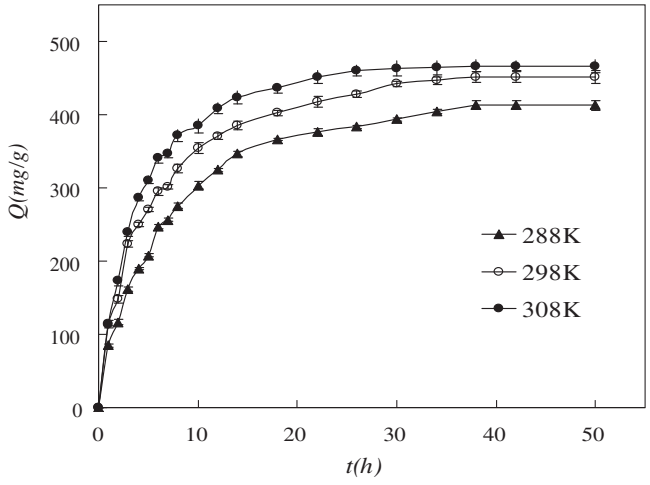

Fig. 5. Adsorption kinetics and capacity Q at different times and different temperatures (resin 15.0 mg, $[Hg^{2+}]_0$ = 10.0 mg/30.0 mL, pH 6.5, 100 rpm).

3.6. Isotherm of adsorption

The adsorption isotherms describe the relationship between the concentration of metal ion in solution and the amount of metal ion adsorbed on the adsorbent at a constant temperature. Collected adsorption data at three constant temperatures in the preferred pH of 6.5 were fitted with three common adsorption models: Langmuir [35], Freundlich [36], and Dubinin-Radushkevich (D-R) [37] isotherm models. The Langmuir isotherm model was developed to describe the adsorption process occurred on the adsorbents with homogeneous and flat surface. The model assumes that each adsorptive site can only be occupied once in a one-on-one manner. The linear form of the Langmuir equation is formulated as follows:

$$\frac{C_e}{Q_e} = \frac{C_e}{Q_m} + \frac{1}{K_L Q_m} \tag{9}$$

where Q_e (mg/g) is the equilibrium adsorption capacity, C_e (mg/mL) is the equilibrium concentration, Q_m (mg/g) is the maximum adsorption capacity of Langmuir, K_L (mL/mg) is Langmuir constant related to the energy of adsorption and increases with the increasing strength of the adsorption bond, which is used to evaluate the dimensionless parameter known as separation factor (R_L) using the equation [38]:

$$R_L = \frac{1}{1 + K_L C_0} \tag{10}$$

where C_0 is the initial concentration of Hg(II), R_L depicts whether the monolayer adsorption predicted by the Langmuir model is irreversible ($R_L = 0$), favorable ($0 < R_L < 1$), linear($R_L = 1$), or unfavorable ($R_L > 1$). The calculated values of R_L were between 0 and 1 (Table 4), indicating that the adsorption of Hg(II) on PAN-ATD is favorable. The Freundlich isotherm model, on the other hand, is used to describe the adsorption process occurred on the adsorbents with heterogeneous surfaces. The linear form of the Freundlich model equation is expressed as follows:

Table 3
Kinetic parameters for Hg(II) adsorption by PAN-ATD.

	Q_e (mg/g)	k_1 (min^{-1})×10^3	Q_1 (mg/g)	R^2
Pseudo-first-order				
288 K	412.8 ± 6.2	1.72 ± 0.03	337.4 ± 5.8	0.9851 ± 0.002
298 K	451.4 ± 7.6	1.87 ± 0.05	343.9 ± 6.9	0.9779 ± 0.001
308 K	466.6 ± 8.0	2.55 ± 0.06	371.0 ± 8.2	0.9910 ± 0.0003
	Q_e (mg/g)	k_2 (g/(mg min))×10^3	Q_2 (mg/g)	R^2
Pseudo-second-order				
288 K	412.8 ± 6.2	2.13 ± 0.02	470.0 ± 6.3	0.9990 ± 0.0003
298 K	451.4 ± 7.6	2.01 ± 0.04	496.5 ± 6.8	0.9995 ± 0.0004
308 K	466.6 ± 8.0	1.97 ± 0.03	508.6 ± 8.7	0.9994 ± 0.0004
	Q_e (mg/g)	α (mg/g min)	β (g/mg) × 10^2	R^2
Elovich				
288 K	412.8 ± 6.2	3.38 ± 0.05	1.05 ± 0.05	0.9802 ± 0.004
298 K	451.4 ± 7.6	5.63 ± 0.07	1.07 ± 0.06	0.9774 ± 0.006
308 K	466.6 ± 8.0	7.75 ± 0.13	1.07 ± 0.07	0.9436 ± 0.006

Table 4
Isotherm parameters for Hg(II) adsorption by PAN-ATD.

	Q_m (mg/g)	K_L (mL/mg)	R_L	R^2
Langmuir				
288 K	484.5 ± 9.1	63.3 ± 2.0	0.0327–0.0559	0.9984 ± 0.0005
298 K	511.2 ± 8.4	81.8 ± 1.9	0.0255–0.0438	0.9965 ± 0.0005
308 K	526.9 ± 7.5	69.9 ± 1.7	0.0297–0.0509	0.9972 ± 0.0004
		$1/n$	K_f ((mg/g)/(mg/mL)$^{1/n}$)	R^2
Freundlich				
288 K		0.13 ± 0.02	558.3 ± 8.6	0.9305 ± 0.0008
298 K		0.12 ± 0.03	590.2 ± 9.3	0.8627 ± 0.0009
308 K		0.11 ± 0.01	601.2 ± 8.4	0.9522 ± 0.0008
		β (mol^2/J^2) × 10^9	Q_m (mg/g)	R^2
D–R				
288 K		5.1 ± 0.23	492.7 ± 4.6	0.9515 ± 0.003
298 K		4.2 ± 0.53	507.8 ± 6.7	0.8799 ± 0.001
308 K		3.7 ± 0.25	528.5 ± 5.1	0.9084 ± 0.004

$$\log Q_e = \log K_f + \frac{1}{n}\log C_e \quad (11)$$

where Q_e, C_e is defined as above, $1/n$ is an empirical parameter involves the adsorption intensity, which varies with the heterogeneity of material, and K_f is roughly an indicator of the adsorption capacity. Unlike the Langmuir and Freundlich isotherms models, the D-R isotherm is commonly employed to specify the nature of adsorption process through physisorption or chemisorptions. It can be used to describe the adsorption process occurred on both homogeneous and heterogeneous surfaces. The linear form of this model can be represented as:

$$\ln Q_e = \ln Q_m - \beta\varepsilon^2 \quad (12)$$

where Q_e is the amount of adsorbed Hg(II) per unit adsorbent (mg/g), Q_m is the calculated adsorption capacity, β is activity coefficient pertinent to mean adsorption energy, and ε is Polanyi potential, which can be calculated through:

$$\varepsilon = RT\ \ln(1 + 1/C_e) \quad (13)$$

Mean adsorption energy, E (kJ/mol), is very useful to determine the mechanisms of adsorption process, which can be expressed as the following equation:

$$E = 1/\sqrt{2\beta} \quad (14)$$

The E value between 8 and 16 kJ/mol means the type of adsorption process is chemical, however, if $E < 8$ kJ/mol, the process is physical. The values of E (kJ/mol) (288 K, 9.9; 298 K, 10.91; 308 K, 11.62) were founded to be above 8 kJ/mol, indicating that the Hg(II) adsorption on PAN-ATD is a chemical process. The isotherm constants as well as the correlation coefficients (R^2) were computed and listed in Table 4. After comparing the three theoretical models to the experimental data, it can easily be found that the Langmuir model was best fitted to the experiment results over the other isotherms, demonstrating that the adsorption of Hg(II) on PAN-ATD is of a monolayer type where interactions between adsorbed molecules are negligible [39].

3.7. Adsorption thermodynamic

The thermodynamic feasibility and the nature of the adsorption process were further investigated by allowing 15 mg PAN-ATD to equilibrate with 30 mL of Hg(II) solutions (10 mg/30 mL) under 288, 298, and 308 K with an initial solution pH of 6.5. The thermodynamic parameters: Gibbs free energy (ΔG), enthalpy (ΔH), and entropy (ΔS) can be calculated using the following equations [40]:

Table 5
Reusing the PAN-ATD for the adsorption of Hg(II).

Hg(II)	Adsorption capacity(mg/g)				
	First time	Second time	Third time	Fourth time	Fifth time
	447.8 ± 6.1	430.7 ± 5.7	423.7 ± 5.3	400.9 ± 4.9	381.6 ± 7.1

Table 6
Adsorption capacities of different adsorbents.

Adsorbents	Adsorption capacities (mg/g)	Desorption ratio	Refs.
2-(Chloromethyl) benz-imidazole modified chitosan	257.8	100	[5]
2-Aminothiazol modified polyacrylonitrile	454.9	100	[22]
Chitosan-poly(vinyl alcohol)	585.9	47	[44]
Multi-cyanoguanidine modified magnetic chitosan	285.7	–	[45]
Sulfamine modified chloromethylated polystyrene	222.2	–	[46]
Brazilian pepper biochars	15.1–24.2	–	[47]
LPSSF modified Na-montmorillonite clays(LPSSF means lipopeptides produced from solid-state fermentation)	38.2–49.1	80	[48]
Mercapto-functionalized core–shell structured nano-magnetic Fe_3O_4 polymers	129.9–256.4	–	[49]
Triethylenetetramine bis (methylene phosphonic acid) modified silica gel	303.0	–	[50]
PAN–ATD	526.9	100	This work

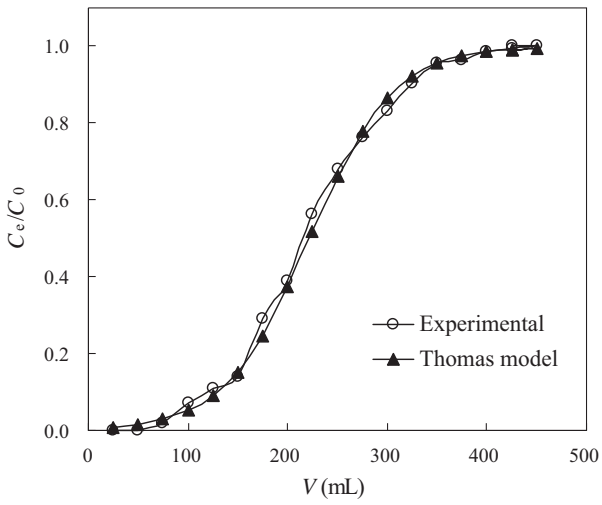

Fig. 6. Experimental and predicted breakthrough curves using Thomas model for Hg(II) adsorption by PAN-ATD (resin 100.0 mg, pH 6.5, C_0 = 0.20 mg/mL, flow rate = 0.25 mL/min).

$$\log D = -\frac{\Delta H}{2.303RT} + \frac{\Delta S}{2.303R} \quad (15)$$

$$\Delta G = \Delta H - T\Delta S \quad (16)$$

where D is the distribution coefficient, R is the gas constant (8.314 J/(mol K)), and T is the absolute temperature (K). The ΔG is a fundamental criterion to determine if a process occurs spontaneously. The negative value of ΔG (kJ/mol) (288 K, -21.6; 298 K, -23.1;

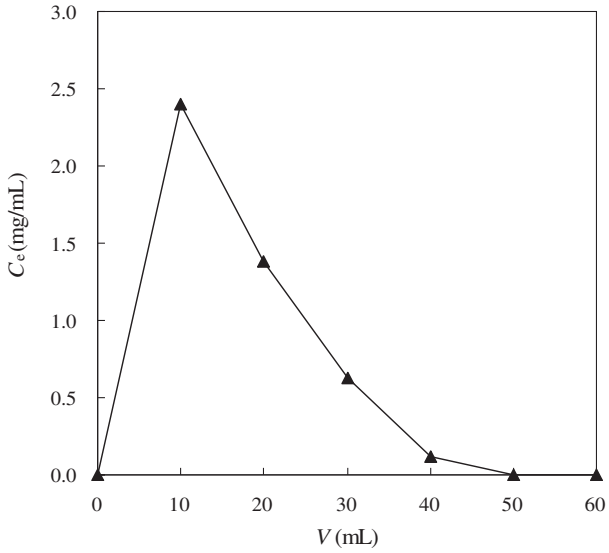

Fig. 7. Dynamic desorption curve flow rate = 0.1 mL/min.

308 K, -24.7) indicates that the Hg(II) adsorption process on the PAN-ATD is feasible and spontaneous. The decrease in magnitude of ΔG as temperature rises from 288 K to 318 K confirms that the adsorption is more favored at higher temperatures. Enhancement of adsorption capacity of PAN-ATD at higher temperatures may be attributed to the greater swelling of the resin and increased diffusion of metal ions into the resin [41]. The positive value of ΔH = 22.2 kJ/mol suggests that the Hg(II) adsorption is an endothermic process, and since the adsorption capacity increases with temperature, one can say that chemisorption process is significant and rate controlling [42], which is agree with the result of kinetics study. In addition, the positive value of ΔS = 152.4 J/(K mol) confirms that the randomness increased at the solid-solution interface during the fixation of Hg(II) ion PAN-ATD surface, which suggests that the adsorption is an entropy-driven process [43].

3.8. Desorption and regeneration studies

To reduce the cost of removal process, the desorption and regeneration of Hg(II) from the resin is necessary. Hg(II) saturated PAN-ATD were eluted with 30 mL HCl and HNO_3 in various concentrations (0.5–4.0 mol/L) under 100 rpm at 298 K for 24 h, respectively. The desorption data shows that the adsorbed Hg(II) can be completely desorbed by 4 mol/L HCl or HNO_3 solution with a desorption ratio of 100%. To determine the reusability of the PAN-ATD, consecutive adsorption–desorption cycles were repeated five times using the same beads. The results of the five adsorption–desorption cycles are shown in Table 5, indicating that the adsorption capacity was barely affected during the repeated adsorption–desorption operations and the adsorption capacity was maintained at 90.8% after five cycles. These results suggests that PAN-ATD could be repeatedly used in the enhanced removal of Hg(II) from waste solution.

Data on the adsorption capacity and desorption ratio of Hg(II) by the recent reported adsorbents [5,22,44–50] were listed in Table 6. Though some materials exhibit a higher adsorption capacity of Hg(II), the PAN-ATD with a good overall property (a high adsorption capacity and a 100% desorption ratio) used for Hg(II) removal is still very attractive.

3.9. Column studies

3.9.1. Dynamic adsorption curve

Compared with the batch experiments, column adsorption tests for the absorbents is more meaningful in practical application. The

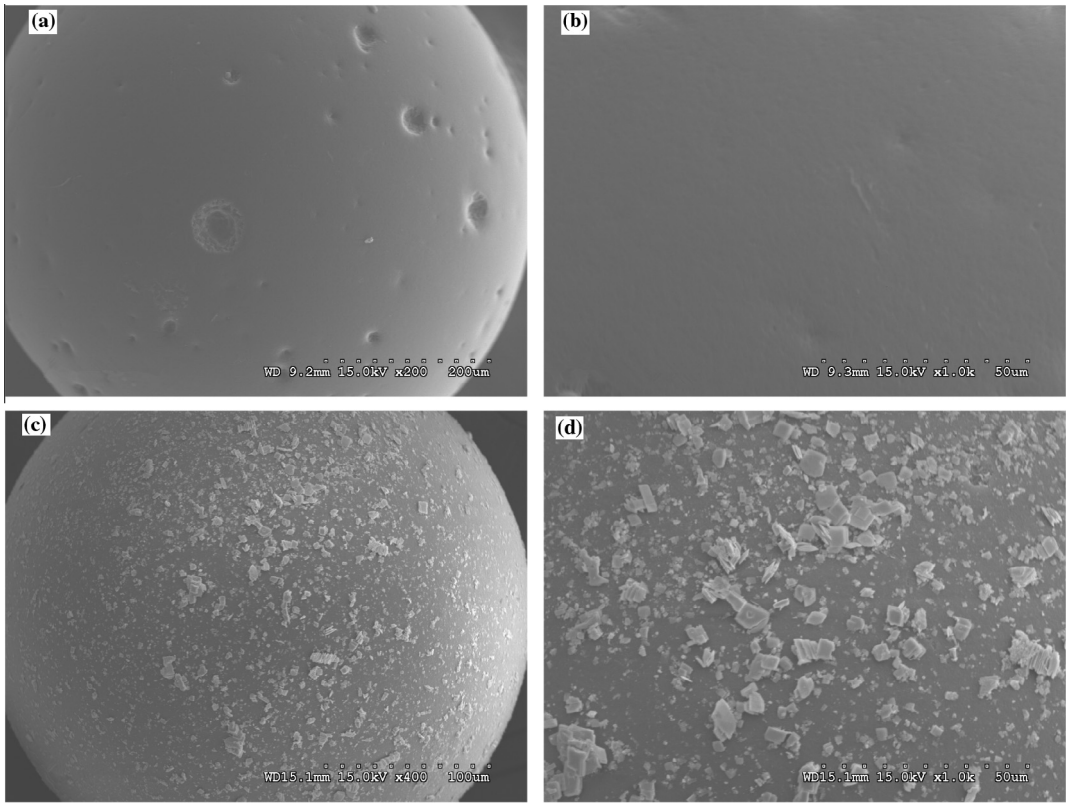

Fig. 8. SEM images of PAN-ATD (a, b) and Hg(II)-loaded PAN-ATD (c, d).

breakthrough analysis was usually applied to investigate the efficiency of the column adsorption process [51]. The adsorption capacity of Hg(II) (Q, mg/g) in the column for a given feed concentration and flow rate can be calculated from

$$Q = \int_0^v \frac{(C_0 - C_e)}{m} dV \quad (17)$$

where C_0 and C_e are metal ion concentrations in the influent and effluent (mg/mL), respectively, m is the total weight of the sorbent loaded in the column, and V is the volume of metal solution passed through the column (mL). The capacity value Q was obtained by graphical integration as 459.5 mg/g. Successful design of a column sorption process requires prediction of the concentration–time profile or breakthrough curve for the effluent. Traditionally, the Thomas model is used to fulfill the purpose. The model has the following form:

$$\frac{C_e}{C_0} = \frac{1}{1 + \exp[K_T(Qm - C_0)/\theta]} \quad (18)$$

where K_T is the Thomas rate constant (mL/(min mg)), θ is the volumetric flow rate (mL/min), and m is the mass of the resin (g). The linearized form of the Thomas model is as follows:

$$\ln\left(\frac{C_0}{C_e} - 1\right) = \frac{K_T Q m}{\theta} - \frac{K_T C_0}{\theta} V \quad (19)$$

The kinetics coefficient K_T and the adsorption capacity Q of the column can be determined from a plot of $\ln[(C_0/C_e) - 1]$ versus t at a certain flow rate. The Thomas equation coefficient for Hg(II) adsorption was $K_T = 1.63 \times 10^{-2}$ mL/(mg min) and $Q = 485.8$ mg/g. The theoretical predictions based on the model parameters were compared with the observed data as shown in Fig. 6. Considering the high R^2 value (0.9983) and the good agreement of the calculated Q with the experimental data, the Thomas model can be applied to design and simulate column adsorption process.

3.9.2. Dynamic desorption curve

With respect to the dynamic desorption of Hg(II) from PAN-ATD, the 4.0 mol/L HNO_3 eluent was employed. The desorption curve was plotted with the effluent concentration (C_e) versus elution volume (V) from the column at a flow rate of 0.1 mL/min. As shown in Fig. 7, a sharp increase of Hg(II) concentration at the beginning of acid elution was observed and 50 mL 4.0 mol/L HNO_3 eluent solution provided effectiveness of the desorption of Hg(II) from PAN-ATD, after which further desorption is negligible.

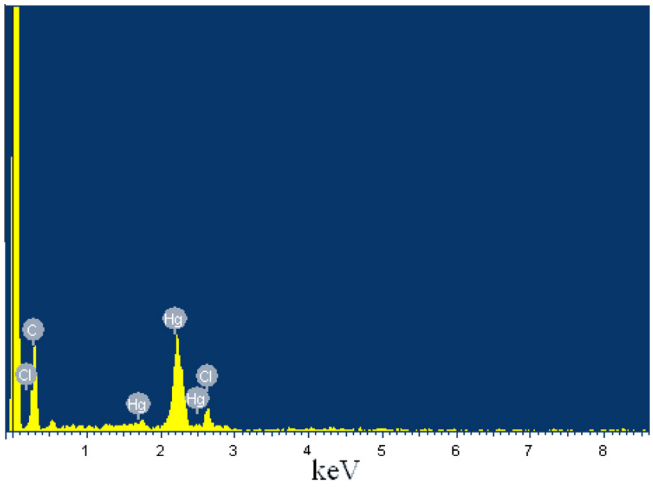

Fig. 9. EDS spectrum of Hg(II)-loaded PAN-ATD.

3.10. SEM and EDS analysis

The morphologies and surface compositions of PAN-ATD before and after Hg(II) adsorption were characterized by SEM and shown in Fig. 8. Apparently, the smooth surface of PAN-ATD turned thicker and coarser with granular flake material after adsorption of Hg(II), which suggested that the mercury was loaded on the surface of the resin. In addition, the presence of the peak of mercury in the EDS spectra in Fig. 9 further confirmed this fact.

4. Conclusions

A novel chelating resin, PAN-ATD, was successfully synthesized by grafting 2-amino-1,3,4-thiadiazole on the surface of polyacrylonitrile beads via one-step reaction. Batch adsorption results showed that the resin possess an excellent selective adsorption ability of Hg(II) in the mixed metal solutions containing Hg(II), Ni(II), Cu(II), Cd(II), Pb(II), and Zn(II) metal ions. FT-IR analysis revealed that the nitrogens in –N–H, C–N, C=N and —C=NH contributed to the adsorption of Hg(II). The adsorption process follows pseudo-second-order model, suggesting that chemisorption is the rate-controlling step. The well fits to the Langmuir isotherm indicates that the monolayer adsorption is dominant. Thermodynamic parameters obtained suggest that Hg(II) adsorbed on PAN-ATD is spontaneous and endothermic in nature. Complete desorption of Hg(II) was achieved by using 4 mol/L HCl or HNO_3 solution, and the regenerated adsorbents could be reused with little loss of adsorption capacity. Therefore, the resin can not only be used in selective removal of Hg(II) from waste solution, but also can be applied in the area of analysis and detection.

Acknowledgments

The work is supported by the National Natural Science Foundation of China (No. 21276235), Ph.D. Programs Foundation of Ministry of Education of China (No. 20133326110006), Funds of Zhejiang Provincial Key Lab. of Industrial Textile Materials & Manufacturing Tech.

Appendix A. Supplementary data

Supplementary data associated with this article can be found, in the online version, at http://dx.doi.org/10.1016/j.cej.2014.07.114.

References

[1] D.W. O'Connell, C. Birkinshaw, T.F. O'Dwyer, Heavy metal adsorbents prepared from the modification of cellulose: a review, Bioresour. Technol. 99 (2008) 6709–6724.
[2] H. Javadian, M. Ghaemy, M. Taghavi, Adsorption kinetics, isotherm, and thermodynamics of Hg^{2+} to polyaniline/hexagonal mesoporous silica nanocomposite in water/wastewater, J. Mater. Sci. 49 (2014) 232–242.
[3] J.H. Yuan, R.K. Xu, H. Zhang, The forms of alkalis in the biochar produced from crop residues at different temperatures, Bioresour. Technol. 102 (2011) 3488–3497.
[4] T.A. Kurniawan, G.Y.S. Chan, W.H. Lo, S. Babel, Physicochemical treatment techniques for wastewater laden with heavy metals, Chem. Eng. J. 118 (2006) 83–98.
[5] C.H. Xiong, L.L. Pi, X.Y. Chen, L.Q. Yang, C.A. Ma, X.M. Zheng, Adsorption behavior of Hg^{2+} in aqueous solutions on a novel chelating cross-linked chitosan microsphere, Carbohydr. Polym. 98 (2013) 1222–1228.
[6] A. Sari, M. Tuzen, Removal of mercury(II) from aqueous solution using moss (*Drepanocladus revolvens*) biomass: equilibrium, thermodynamic and kinetic studies, J. Hazard. Mater. 171 (2009) 500–507.
[7] P.H. Chen, C.F. Hsu, D.D.W. Tsai, Y.M. Lu, W.J. Huang, Adsorption of mercury from water by modified multi-walled carbon nanotubes: adsorption behaviour and interference resistance by coexisting anions, Environ. Technol. 35 (2014) 1935–1944.
[8] M. Hadavifara, N. Bahramifar, H. Younesi, Q. Li, Adsorption of mercury ions from synthetic and real wastewater aqueous solution by functionalized multi-

walled carbon nanotube with both amino and thiolated groups, Chem. Eng. J. 237 (2014) 217–228.
[9] T.Y. Liu, Z.L. Wang, X.X. Yan, B. Zhang, Removal of mercury (II) and chromium (VI) from wastewater using a new and effective composite: pumice-supported nanoscale zero-valent iron, Chem. Eng. J. 245 (2014) 34–40.
[10] S. Thakur, S. Kumari, P. Dogra, G.S. Chauhan, A new guar gum-based adsorbent for the removal of Hg(II) from its aqueous solutions, Carbohydr. Polym. 106 (2014) 276–282.
[11] H. Javadian, M. Taghavi, Application of novel Polypyrrole/thiol-functionalized zeolite Beta/MCM-41 type mesoporous silica nanocomposite for adsorption of Hg^{2+} from aqueous solution and industrial wastewater: kinetic, isotherm and thermodynamic studies, Appl. Surf. Sci. 289 (2014) 487–494.
[12] N. Saman, K. Johari, H. Mat, Adsorption characteristics of sulfur-functionalized silica microspheres with respect to the removal of Hg(II) from aqueous solutions, Ind. Eng. Chem. Res. 53 (2014) 1225–1233.
[13] S.A. El-Safty, Organic–inorganic hybrid mesoporous monoliths for selective discrimination and sensitive removal of toxic mercury ions, J. Mater. Sci. 44 (2009) 6764–6774.
[14] S. Kagaya, H. Miyazaki, M. Ito, K. Tohda, T. Kanbara, Selective removal of mercury (II) from waste water using polythioamides, J. Hazard. Mater. 175 (2010) 1113–1115.
[15] X.M. Sun, R.J. Qu, C.M. Sun, Ying Zhang, S.H. Sun, C.N. Ji, Ping Yin, Sol–gel preparation and Hg(II) adsorption properties of silica-gel supported low generation polyamidoamine dendrimers polymer adsorbents, Ind. Eng. Chem. Res. 53 (2014) 2878–2888.
[16] F. Raji, M. Pakizeh, Kinetic and thermodynamic studies of Hg(II) adsorption onto MCM-41 modified by $ZnCl_2$, Appl. Surf. Sci. 301 (2014) 568–575.
[17] T. Sheela, Y.A. Nayaka, R. Viswanatha, S. Basavanna, T. Venkatesha, Kinetics and thermodynamics studies on the adsorption of Zn(II), Cd(II) and Hg(II) from aqueous solution using zinc oxide nanoparticles, Powder Technol. 217 (2012) 163–170.
[18] S.N. Azizi, A.R. Dehnavi, A. Joorabdoozha, Synthesis and characterization of LTA nanozeolite using barley husk silica: mercury removal from standard and real solutions, Mater. Res. Bull. 48 (2013) 1753–1759.
[19] P. Figueira, C.B. Lopes, A.L. Daniel-da-Silva, E. Pereira, A.C. Duarte, T. Trindade, Removal of mercury(II) by dithiocarbamate surface functionalized magnetite particles: application to synthetic and natural spiked waters, Water Res. 45 (2011) 5773–5784.
[20] S. Deng, R. Bai, J.P. Chen, Aminated polyacrylonitrile fibers for lead and copper removal, Langmuir 19 (2003) 5058–5064.
[21] S. Deng, R. Bai, Removal of trivalent and hexavalent chromium with aminated polyacrylonitrile fibers: performance and mechanisms, Water Res. 38 (2004) 2424–2432.
[22] C.H. Xiong, Q. Jia, X.Y. Chen, G.T. Wang, C.P. Yao, Optimization of polyacrylonitrile-2-aminothiazole resin synthesis, characterization, and its adsorption performance and mechanism for removal of Hg(II) from aqueous solutions, Ind. Eng. Chem. Res. 52 (2013) 4978–4986.
[23] G.R. Kiani, H. Sheikhloie, N. Arsalani, Heavy metal ion removal from aqueous solutions by functionalized polyacrylonitrile, Desalination 269 (2011) 266–270.
[24] L.G. Han, Y.P. Tao, H.Q. Liang, Z.J. Liu, Raman, FT-IR spectra, DFT calculation and normal mode analysis of 2-mercapto-thiadiazole, Chin. J. Light Scattering 22 (2010) 6–10.
[25] X.L. Dong, L.Q. Ma, Y.J. Zhu, Y.C. Li, B.H. Gu, Mechanistic investigation of mercury sorption by brazilian pepper biochars of different pyrolytic temperatures based on X-ray photoelectron spectroscopy and flow calorimetry, Environ. Sci. Technol. 47 (2013) 12156–12164.
[26] Y.Y. Chen, Y. Zhao, Synthesis and characterization of polyacrylonitrile-2-amino-2-thiazoline resin and its sorption behaviors for noble metal ions, React. Funct. Polym. 55 (2003) 89–98.
[27] L. García-Río, J.R. Leis, J.A. Moreira, E. Araujo, F. Norberto, L. Ribeiro, Mechanism for basic hydrolysis of N-Nitrosoguanidines in aqueous solution, J. Org. Chem. 68 (2003) 4330–4337.
[28] E. Guibal, Interactions of metal ions with chitosan-based sorbents: a review, Sep. Purif. Technol. 38 (2004) 43–74.
[29] J. Wang, B.L. Deng, H. Chen, X.R. Wang, J.Z. Zheng, Removal of aqueous Hg(II) by polyaniline: sorption characteristics and mechanisms, Environ. Sci. Technol. 43 (2009) 5223–5228.
[30] R.S. Vieiraa, M.L.M. Oliveirab, E. Guibalc, E. Rodríguez-Castellónb, M.M. Beppu, Copper mercury and chromium adsorption on natural and crosslinked chitosan films: an XPS investigation of mechanism, Colloid Surf. A 374 (2011) 108–114.
[31] Y.S. Ho, G. McKay, A comparison of chemisorption kinetic models applied to pollutant removal on various sorbents, Process Saf. Environ. Prot. 76 (1998) 332–340.
[32] Y.S. Ho, Removal of copper ions from aqueous solution by tree fern, Water Res. 37 (2003) 2323–2330.
[33] K. Aparecida, G. Gusmao, L.V.A. Gurgel, T.M.S. Melo, F. Gil, Application of succinylated sugarcane bagasse as biosorbent to remove methylene blue and gentian violet from aqueous solutions—kinetic and equilibrium studies, Dyes Pigments 92 (2012) 967–974.
[34] M. Monier, D.A. Abdel-Latif, Modification and characterization of PET fibers for fast removal of Hg(II), Cu(II) and Co(II) metal ions from aqueous solutions, J. Hazard. Mater. 122 (2013) 250–251.
[35] I. Langmuir, Adsorption of gases on plain surface of glass mica platinum, J. Am. Chem. Soc. 40 (1918) 1361–1403.
[36] H.M.F. Freundlich, Über die adsorption in lösungen, Z. Phys. Chem. 57 (1906) 385–470.
[37] M.M. Dubinin, L.V. Radushkevich, Equation of the characteristic curve of activated charcoal, Chem. Zentralbl. 1 (1947) 875.
[38] V.M. Boddu, K. Abburi, J.L. Talbott, E.D. Smith, R. Haasch, Removal of arsenic (III) and arsenic (V) from aqueous medium using chitosan-coated biosorbent, Water Res. 42 (2008) 633–642.
[39] A.R. Ghenberpour, Simple Kinetics of Reactions, Tehran University Press, Tehran, 1986.
[40] L.C. Zheng, Z. Dang, X.Y. Yi, H. Zhang, Equilibrium and kinetic studies of adsorption of Cd(II) from aqueous solution using modified corn stalk, J. Hazard. Mater. 176 (2010) 650–656.
[41] C.H. Xiong, S.G. Zhou, X.Z. Liu, Q. Jia, C.A. Ma, X.M. Zheng, 2-Aminothiazole functionalized polystyrene for selective removal of Au(III) in aqueous solutions, Ind. Eng. Chem. Res. 53 (2014) 2441–2448.
[42] D.M. Danijela, B.N. Aleksandra, D.M.-N. Aleksandra, T.S. Ljiljana, P.S. Zvjezdana, V.H. Radmila, E.O. Antonije, Equilibrium and kinetics study on hexavalent chromium adsorption onto diethylene triamine grafted glycidyl methacrylate based copolymers, J. Hazard. Mater. 209–210 (2012) 99–110.
[43] J. Wu, Z.W. Xu, W.M. Zhang, L. Lv, B.C. Pan, G.Z. Nie, M.H. Li, Q. Du, Application of heterogeneous adsorbents in removal of dimethyl phthalate: equilibrium and heat, AICHE J. 56 (2010) 2699–2705.
[44] X.H. Wang, W.Y. Deng, Y.Y. Xie, C.Y. Wang, Selective removal of mercury ions using a chitosan–poly(vinyl alcohol) hydrogel adsorbent with three-dimensional network structure, Chem. Eng. J. 228 (2013) 232–242.
[45] Y. Wang, Y.X. Qi, Y.F. Li, J.J. Wu, X.J. Ma, C. Yu, L. Ji, Preparation and characterization of a novel nano-absorbent based on multi-cyanoguanidine modified magnetic chitosan and its highly effective recovery for Hg(II) in aqueous phase, J. Hazard. Mater. 260 (2013) 9–15.
[46] Y.X. Qi, X.L. Jin, C. Yu, Y. Wang, L.Q. Yang, Y.F. Li, A novel chelating resin containing high levels of sulfamine group: preparation and its adsorption characteristics towards *p*-toluenesulfonic acid and Hg(II), Chem. Eng. J. 233 (2013) 315–322.
[47] X.L. Dong, L.Q. Ma, Y.J. Zhu, Y.C. Li, B.H. Gu, Mechanistic investigation of mercury sorption by brazilian pepper biochars of different pyrolytic temperatures based on X-ray photoelectron spectroscopy and Flow Calorimetry, Environ. Sci. Technol. 47 (2013) 12156–12164.
[48] Z. Zhu, C. Gao, Y.L. Wu, L.F. Sun, X.L. Huang, W. Ran, Q.R. Shen, Removal of heavy metals from aqueous solution by lipopeptides and lipopeptides modified Na-montmorillonite, Bioresour. Technol. 147 (2013) 378–386.
[49] S.D. Pan, Y. Zhang, H.Y. Shen, M.Q. Hu, An intensive study on the magnetic effect of mercapto-functionalized nano-magnetic Fe_3O_4 polymers and their adsorption mechanism for the removal of Hg(II) from aqueous solution, Chem. Eng. J. 210 (2012) 564–574.
[50] Z.D. Wang, P. Yin, Z. Wang, R.J. Qu, X.G. Liu, Chelating resins silica gel supported aminophosphonic acids prepared by a heterogeneous synthesis method and a homogeneous synthesis method and the removal properties for Hg(II) from aqueous solutions, Ind. Eng. Chem. Res. 51 (2012) 8598–8607.
[51] N.H. Mthombeni, L. Mpenyana-Monyatsi, M.S. Onyango, M.N. Momba, Breakthrough analysis for water disinfection using silver nanoparticles coated resin beads in fixed-bed column, J. Hazard. Mater. 217–218 (2012) 133–140.